XLI CILAMCE
XLI Ibero-Latin American Congress on Computational Methods in Engineering
16-19 November, 2020 FOZ DO IGUAÇU PARANÁ - BRAZIL

Computational modeling of deformation bands in a plug scale

Renan S. B. de Lima[1,2], Roberto Quevedo[2], Deane Roehl[1,2]

[1]*Civil Engineering Department, PUC-Rio*
Rua Marquês de São Vicente, 225, 22453-900, Rio de Janeiro, Brazil
renanlima@aluno.puc-rio.br, droehl@puc-rio.br
[2]*Tecgraf Institute, PUC-Rio*
Rua Marquês de São Vicente, 225, 22453-900, Rio de Janeiro, Brazil
renanlima@tecgraf.puc-rio.br, rquevedo@tecgraf.puc-rio.br, deane@tecgraf.puc-rio.br

Abstract. The strain localization phenomenon consists in the occurrence of narrow regions due to inelastic deformations and irreversible phenomena. By porous materials such as soils and rocks, localized deformation can affect the integrity and contribute to the initiation of structural failure. Typical examples of strain localization in porous materials are the shear bands, which can be observed experimentally in laboratory tests. The formation of shear bands can be represented through numerical models such as the finite element method (FEM). Thus, in this study, we model the occurrence of shear bands at plug scale and perform a sensitivity analysis of the main parameters involved. The Mohr-Coulomb model with strain softening was used to represent the elastoplastic behavior of the materials. Strain softening was implemented through a progressive reduction of the friction angle as a function of the plastic strain. In the results, structural features of the shear bands are analyzed, such as orientation and band width. From the results, it was observed that the dilation angle is directly related to the orientation of the shear band. Also, the Young's modulus exerts significant influence on the width of the band. These analyses also allowed to identify convergence problems and dependence of the results on mesh discretization level. In this work, we also discuss the source of these problems and mention some alternative techniques that have been proposed to overcome such difficulties using FEM.

Keywords: Damage zones, Shear bands, Elastoplastic materials.

1 Introduction

When porous materials are subjected to loads, different mechanisms of deformation occur depending on several conditions such as mineralogy, grain distribution, porosity, mechanical properties, and also on factors including burial depth and stress state history. Under deformation, most porous materials present a transition from elastic to plastic behavior up to reaching a peak in the stress-strain curve, then strains localize in deformation bands, and finally, failure occurs. As a precursor to faulting, understanding deformation bands is fundamental to evaluate their impact on the stability of porous materials. Commonly, deformation bands occur in materials with porosity higher than 15%, such as sandstones but also some limestones and tuffs [1]. The band width is variable, but in general, corresponds to mm-thick zones. Deformation bands can be classified in a kinematic framework, depending on the deformation mechanism into shear bands, dilation bands, and compaction bands.

Many researchers have carried out direct shear, simple shear, hollow cylinder, triaxial, and biaxial tests in order to investigate and characterize strain localization through shear bands [2]. Also, advanced experimental techniques, such as X-ray computed tomography stereophotogrammetry, and particle image velocimetry, are used to investigate the micro-scale information. The Discrete element model (DEM) is also used to model shear bands in crushable and irregularly shaped granular materials associated [3]. Numerical simulations based on the finite element method, the discrete element method, and the material point method, among others, have been used together with different constitutive relationships to model deformation bands [4][5][6]. Among the different approaches, the finite element method (FEM) has been used to represent the onset of shear localization owing to

its capabilities to deal with different geometries and constitutive models. However, to model deformation bands, the conventional continuum theory adopted in the standard FEM presents some drawbacks related to mesh sensitivity. The cause of such a problem is the loss of ellipticity of the equilibrium equation due to excessive concentrated strains. Consequently, the resulting width and orientation of deformation bands can be dependent on the adopted element size [7]. As meshes are refined, plastic strains localize into bands that become narrower and narrower [8]. In order to overcome this problem, several enhanced theories have been proposed, such as non-local continuum theories, higher-order gradient continuum models, micro-polar continuum models, and the inclusion of viscoplastic terms [9]. Such enhanced continuum models can provide the so-called regularization of boundary value problems and simulate shear localization while preserving ellipticity. Other techniques consist of the use of adaptive meshes or the use of alternative approaches such as the Arbitrary Lagrangian-Eulerian (ALE) formulation [10]. However, the development of reliable models capable of capturing the initiation and evolution of deformation bands remains a long-standing challenge [11].

The present work focuses on the simulation of the initiation of shear bands in biaxial compression tests. Several simulations considering the classical continuum formulation with large displacements are performed in order to identify the impact of elastic and strength properties on the initiation of shear bands. The presented results are intended to provide a preliminary qualitative description of the initiation of shear bands and can be used for further analyses considering the listed enhanced techniques.

2 Model description

The model used to represent the initiation of shear bands in a plug scale is shown in Fig. 1. The specimen is 42 mm wide and 84 mm high, as in conventional laboratory tests. Following laboratory tests, the sample is subjected to an initial hydrostatic pressure (σ_c =10 MPa), followed by incremental vertical displacements (U2) imposed to the top up to 19.5 mm. As boundary conditions, the displacements at the specimen base nodes are restricted in both horizontal and vertical directions, while displacements at the nodes of the top are restricted in the horizontal direction. The mechanical behavior of the rock is represented through an elastic-perfectly plastic model considering the Mohr-Coulomb failure criterion. The adopted properties are shown in Tab. 1 and were obtained through laboratory tests carried out in the LEM-DEC Laboratory (PUC-Rio) on Indiana Limestone samples. The finite element mesh is composed of eight-node quadrilateral elements and nine-point Gauss integration.

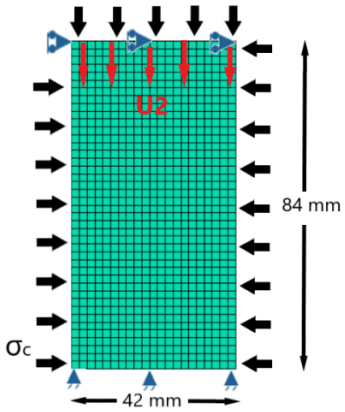

Figure 1. Geometry, mesh, and boundary conditions of finite element models.

Table 1. Properties of the carbonate rock

	Nomenclature	Value
Young's modulus (GPa)	E	20.0
Poisson's ratio (-)	ν	0.25
Cohesion (MPa)	C	5
Friction angle (°)	Φ	35°
Dilation angle (°)	ψ	25°

The simulations were carried out through the Abaqus/Standard® solver. In order to identify the initiation of shear bands, we choose the scalar variable "PEMAG" that represents the magnitude of plastic strain given as:

$$PEMAG = \sqrt{2/3(PE_{P1}{}^2 + PE_{P2}{}^2 + PE_{P3}{}^2)} \quad (1)$$

where $PE_{P1,}$ PE_{P2} and PE_{P3} are the principal plastic strains.

Fig. 2 describes the procedure for measuring the width of the formed shear bands. Along a vertical path created at the bottom right of the models, we measure the evolution of PEMAG and then we define its width, considering the orientation of the shear band.

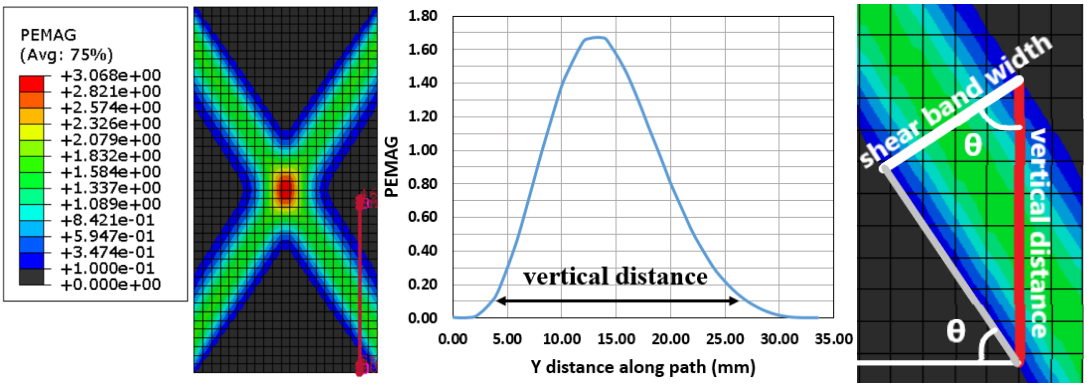

Figure 2. Measurement of the shear band width through PEMAG.

Before performing the sensitivity study, we carried out simulations considering three different discretizations in order to see the effect of the adopted mesh on the results. At each structured mesh, we use element sizes of 1, 2 and 4 mm, obtaining 3528, 882, and 231 quadrilateral elements, respectively. The CPU time spent at each simulation from the least to the most refined mesh was 284.30 s, 66.60 and 18.60 s, respectively. The corresponding contour plots of PEMAG at the end of the three simulations are shown in Fig. 3 for each mesh. We can notice similar orientations but different shear band widths. As meshes are refined, plastic strains localize into narrower bands and with higher values of PEMAG.

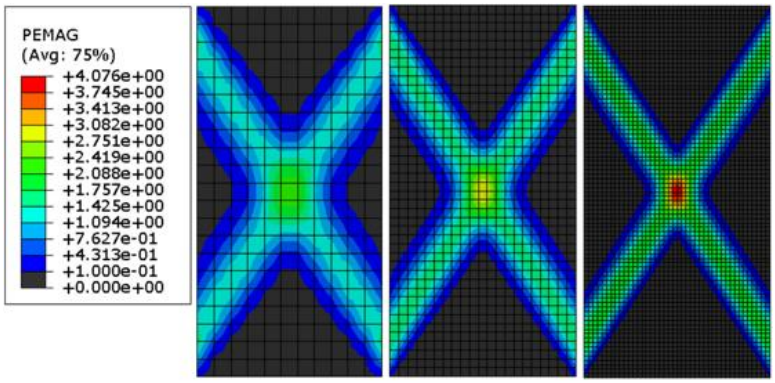

Figure 3. Results obtained with different mesh discretizations. From the left to the right: 4, 2 and 1 mm.

Fig. 4 confirms such visual results through curves of axial strain (ε_a) x deviatoric stress (σ_d) and curves of vertical displacement (D) x shear band width (W). From curve (ε_a x σ_d), we see that plastic deformations initiate for the same value of applied axial deformation (ε_a=0.002and σ_d= 46.2 MPa). However, after that point, the three curves evolve in different ways. We observe that the sample bears relatively higher deviatoric stress when less refined meshes are adopted. From curve (D x W), we notice that at the end of the simulations, larger shear band widths are present, with values of 10, 13, and 16 mm corresponding to meshes with element sizes of 1, 2, and 4

mm, respectively. Those results confirm that the evolution of shear bands is mesh dependent. However, in order to perform a preliminary sensitivity study considering elastic and strength properties, in this study we use the mesh with element sizes of 2 mm for further analyses.

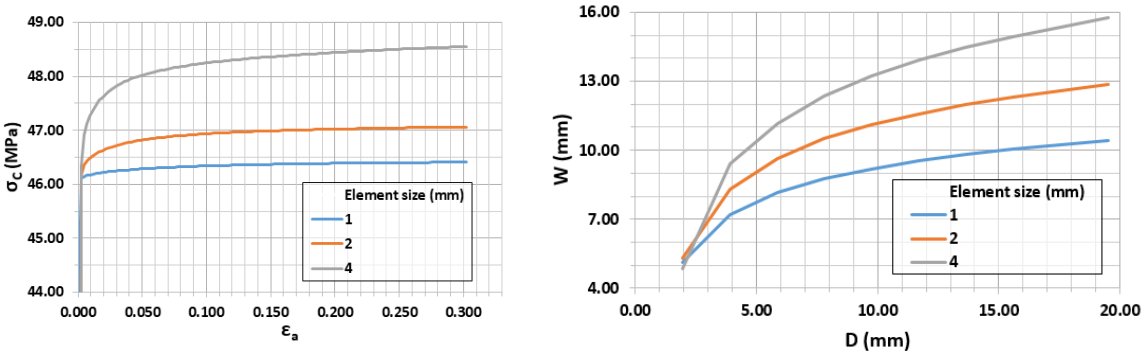

Figure 4. Results obtained in the mesh sensitivity study.

3 Sensitivity study

In this section, we check the influence of the parameters: Young's modulus, Poisson's ratio, friction angle, and dilation angle in the development of the shear band. Furthermore, we also evaluate the impact of softening on the evolution of shear bands. In total 5 sets of simulations were carried out adopting the properties listed on Tab. 1 as reference.

The results for the sensitivity to Young's modulus are shown in Fig. 5. From curve (ε_a x σ_d), we see that stiffer materials bear slightly higher deviatoric stresses. Furthermore, from curve (D x W), we notice that the shear band width increases slightly with the stiffness of the rock.

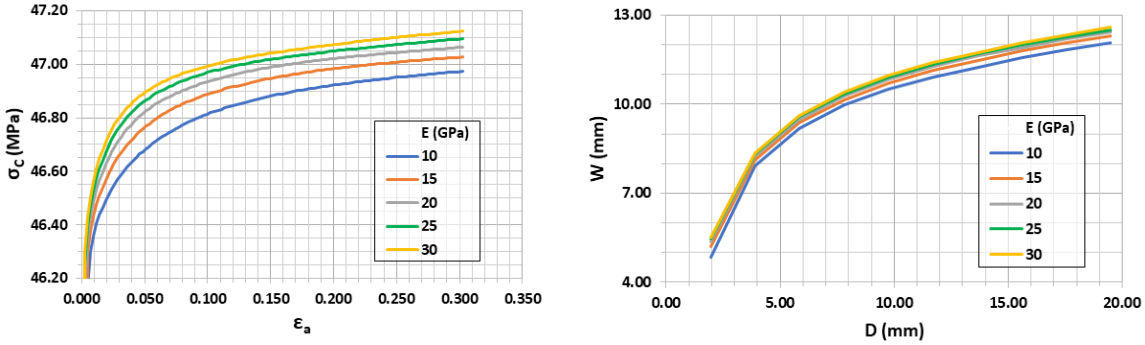

Figure 5. Sensitivity analysis regarding Young's modulus (E).

The results obtained by varying Poisson's ratio are shown in Fig. 6. These results are similar to those found varying Young's modulus and are explained for the same reasons, owing to the occurrence of earlier plastic deformations when Poisson's ratio is higher.

In the next set of simulations, we vary the friction angle from 35 to 25°. In these simulations, we fix the dilation angle at 20° in order to maintain all analyses with a non-associative flow rule. From the results, we can observe that higher deviatoric stresses are reached with higher friction angles. Those results are expected since materials with higher friction angles present larger envelopes, delaying the beginning of plastic deformations. Then, from the WxD plot, we can notice that greater shear band widths are found with lower friction angles.

Next, we fix the friction angle at 35° and vary the dilation angle considering values of 20°, 25°, and 30°. The corresponding results are shown in Fig. 8. Reduced dilation angles limit the evolution of volumetric plastic deformations. From curves (ε_a x σ_d), we can observe that higher deviatoric stresses are present for higher dilation angles. From curves (W x D), we notice that for higher dilation angles, the width of the shear band is smaller. Furthermore, the dilation angle also affects the shear band inclination, as shown in Fig. 9. We notice that higher dilation angles trigger shear band orientations with larger dip angles.

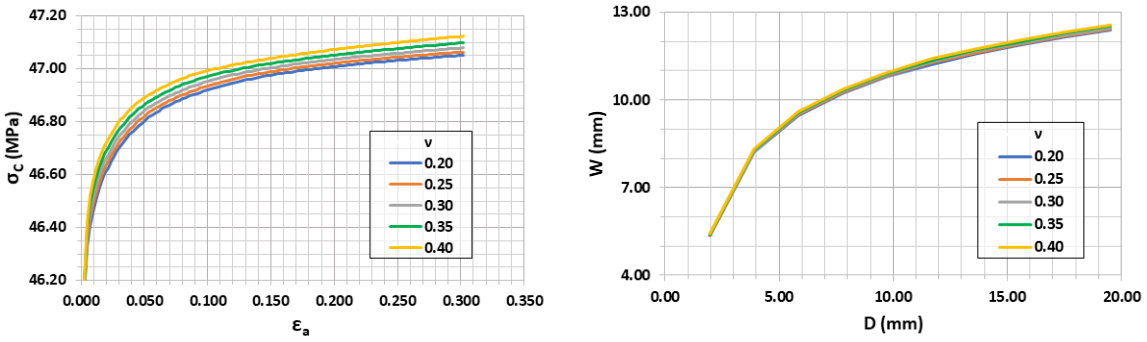

Figure 6. Sensitivity analysis regarding Poisson's ratio (ν).

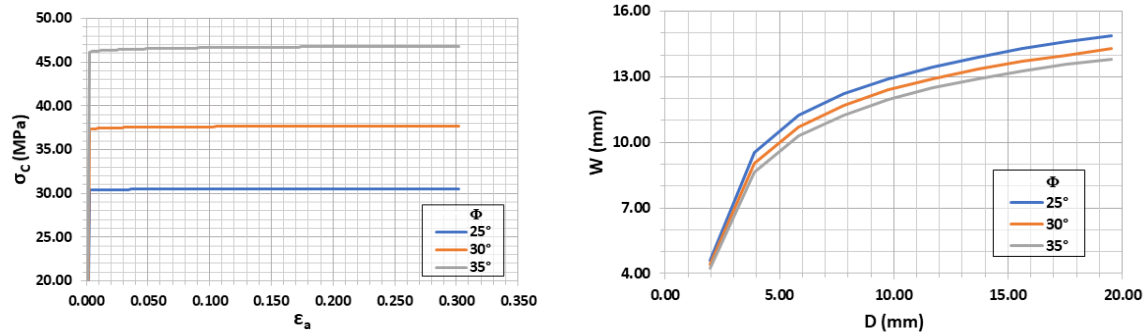

Figure 7. Sensitivity analysis regarding the friction angle (Φ).

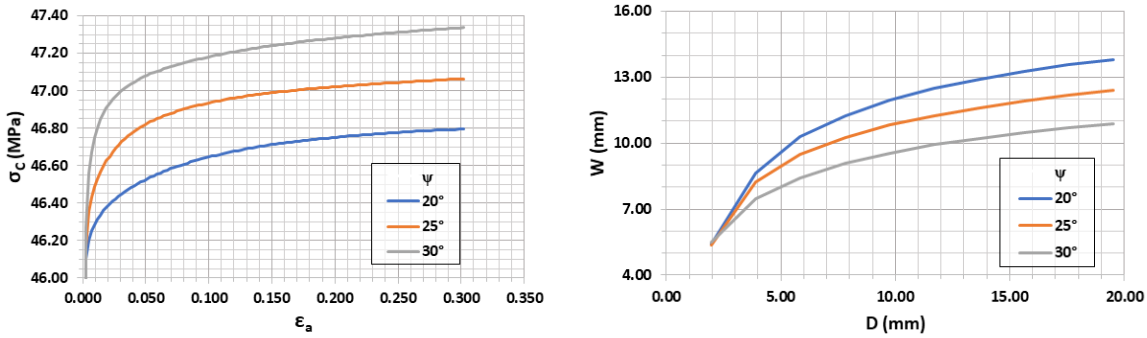

Figure 8. Sensitivity analysis regarding the dilation angle (ψ).

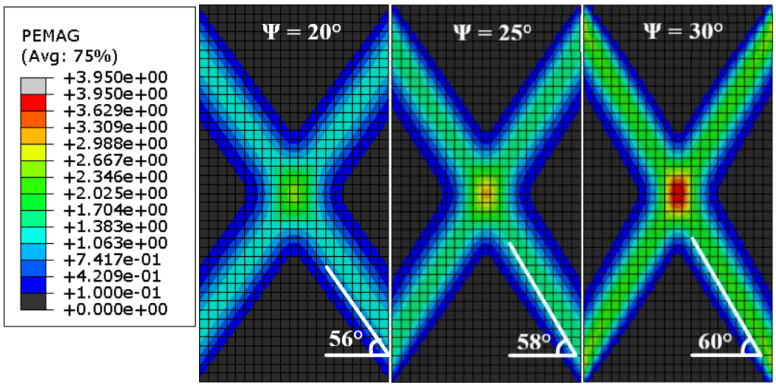

Figure 9. Shear bands obtained for different values of dilation angle (ψ).

In a final set of tests, we include the effect of softening through a reduction of the friction angle with the evolution of PEMAG in the analyses, as shows Fig. 10. In all cases, the dilation angle was kept at 25°, which is the standard value shown in Tab. 1. Fig. 11 presents the corresponding results and compares with the results for perfect plasticity. From curves (ε_a x σ_d), we can observe the significant reduction of the deviatoric stresses with the imposed softening functions. From curves (W x D), we notice that more acute softening triggers narrower shear bands.

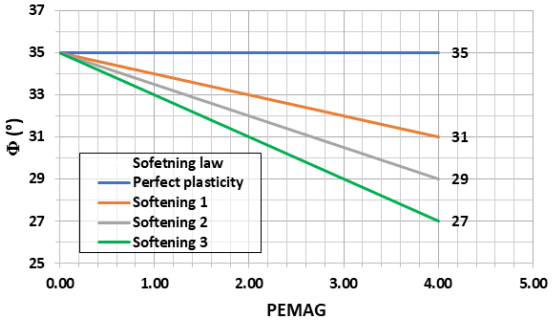

Figure 10. Different softening laws.

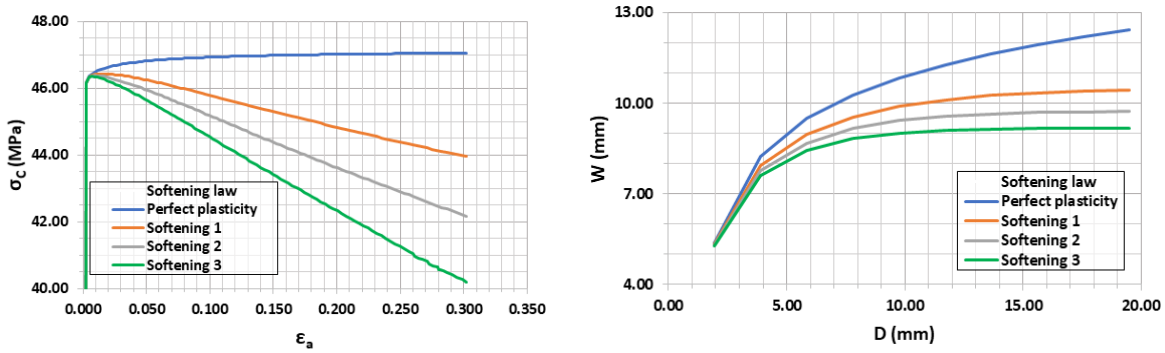

Figure 11. Sensitivity analysis regarding the softening law.

4 Conclusions

In this study, a sensitivity analysis was performed varying the elastic and strength parameters in order to check their impact on the evolution of shear bands in porous materials. Several numerical finite elements models were built using the Mohr Coulomb constitutive model with non-associated plastic flow law. From the results, we observed that the elastic properties (E and ν) can affect the beginning of plastic deformations. However, they do not affect the evolution of shear bands. On the other hand, the evolution of shear bands seems to be sensitive to the adopted strength parameters. From the variation of the friction angle, we observed that lower values trigger earlier plastic deformations and contribute to the development of wide shear bands. From the variation of the dilation angle, we noticed that lower values enable wider shear bands; the friction angle show the same tendency, but more acutely. From the simulations considering softening, we observed that more intense softening contributes to strain localization triggering narrower shear bands. The presented results provide a preliminary and qualitative description of the initiation of shear bands. In further studies, we aim to consider enhanced techniques to avoid mesh dependency and also to include other constitutive models in order to simulate other kinds of deformation bands.

Acknowledgements. This research was carried out in association with the ongoing R&D project registered as ANP n° 21475-9, "GeoBanD – Geomodelagem de zona de dano em falhas geológicas" (PUC-Rio/CENPES/ANP), sponsored by Petrobras. The authors also gratefully acknowledge the support from Coordenação de Aperfeiçoamento de Pessoal de Nível Superior (CAPES).

Authorship statement. The authors hereby confirm that they are the sole liable persons responsible for the authorship of this work, and that all material that has been herein included as part of the present paper is either the property (and authorship) of the authors, or has the permission of the owners to be included here.

5 References

[1] H. Fossen and H. Fossen, "Structural geology and structural analysis," in *Structural Geology*, 2010.

[2] J. Liu, "Numerical investigations of the strain localization in geotechnical engineering within the framework of micropolar theory," École centrale de Nantes, 2018.

[3] W. Zhou, L. Yang, G. Ma, K. Xu, Z. Lai, and X. Chang, "DEM modeling of shear bands in crushable and irregularly shaped granular materials," *Granul. Matter*, vol. 19, no. 2, pp. 1–12, 2017, doi: 10.1007/s10035-017-0712-y.

[4] T. Kiriyama, "Numerical study of shear band formation in triaxial compression tests," *15th Asian Reg. Conf. Soil Mech. Geotech. Eng. ARC 2015 New Innov. Sustain.*, pp. 697–702, 2015, doi: 10.3208/jgssp.JPN-013.

[5] J. Lin and W. Wu, "A comparative study between DEM and micropolar hypoplasticity," *Powder Technol.*, vol. 293, pp. 121–129, 2016, doi: 10.1016/j.powtec.2015.11.033.

[6] R. De Borst, "Simulation of strain localization: A reappraisal of the cosserat continuum," *Eng. Comput.*, vol. 8, no. 4, pp. 317–332, 1991, doi: 10.1108/eb023842.

[7] A. Needleman, "Material rate dependence and mesh sensitivity in localization problems," *Comput. Methods Appl. Mech. Eng.*, vol. 67, no. 1, pp. 69–85, 1988, doi: 10.1016/0045-7825(88)90069-2.

[8] X. Lu, J. P. Bardet, and M. Huang, "Numerical solutions of strain localization with nonlocal softening plasticity," *Comput. Methods Appl. Mech. Eng.*, vol. 198, no. 47–48, pp. 3702–3711, 2009, doi: 10.1016/j.cma.2009.08.002.

[9] A. Noorzad, "Shear Band Formation in Biaxial Compression Test Shear Band Formation in Biaxial Compression Test," no. January 2010, 2015.

[10] X. Wang, D. Chan, and N. Morgenstern, "Numerical modelling of shear bands by element bands," *Int. J. Numer. Methods Eng.*, vol. 54, no. 8, pp. 1131–1159, 2002, doi: 10.1002/nme.464.

[11] L. Berger-Vergiat, X. Chen, and H. Waisman, "Explicit and implicit methods for shear band modeling at high strain rates," *Comput. Mech.*, vol. 63, no. 4, pp. 615–629, 2019, doi: 10.1007/s00466-018-1612-7.